frontiers | Frontiers in Mechanical Engineering

TYPE Original Research
PUBLISHED 22 November 2023
DOI 10.3389/fmech.2023.1286304

OPEN ACCESS

EDITED BY
Majid Baniassadi,
University of Tehran, Iran

REVIEWED BY
Lorenzo Scalera,
University of Udine, Italy
Darryl D'Lima,
Scripps Clinic, United States

*CORRESPONDENCE
Ayu Gareta Risangtuni,
ayugareta@itb.ac.id

RECEIVED 31 August 2023
ACCEPTED 03 November 2023
PUBLISHED 22 November 2023

CITATION
Risangtuni AG, Suprijanto S, Nazaruddin YY and Mahyuddin AI (2023), Dual-mode 3D printed dynamic wrist driven orthosis for hand therapy exercises.
Front. Mech. Eng 9:1286304.
doi: 10.3389/fmech.2023.1286304

Dual-mode 3D printed dynamic wrist driven orthosis for hand therapy exercises

Ayu Gareta Risangtuni*, S. Suprijanto, Yul Yunazwin Nazaruddin and Andi I. Mahyuddin

Engineering Physics Department, Faculty of Industrial Technology, Bandung Institute of Technology, Bandung, Indonesia

The primary objective of the Dual-mode Dynamic Wrist Driven Orthosis (D-WDO) is to facilitate wrist-hand therapy exercises for patients with varying levels of residual muscle function. This dual-mode D-WDO system comprises two main components: the orthosis structure and the soft pneumatic actuator (SPA). All system components were designed and produced using Computer Aided Design (CAD) software and the Fused Deposition Modeling (FDM) 3D printing technique. The D-WDO's structure is constructed from PLA (Polylactic Acid), while the SPA is made from TPU (Thermoplastic Polyurethane) filament. The D-WDO can be operated in passive or active mode by attaching or detaching the SPA from the structure. This D-WDO system is particularly suitable for patients with a minimum MMT level between 2 and 3, as it provides assistance for wrist movement and supports repetitive wrist motion to enhance wrist muscle function. However, it is important to note that the operation and performance of the dual-mode D-WDO system may vary depending on the chosen system configuration. The active D-WDO's performance demonstrates its ability to achieve the necessary wrist flexion angle for a functional wrist joint, especially in the context of daily activities.

KEYWORDS

dynamic wrist-driven orthosis, dual-mode, soft pneumatic actuator, additive manufacturing, hand therapy, repetitive movement

1 Introduction

Humans use their hands to interact with the environment in activities of daily living (ADLs) (Zheng et al., 2013). A healthy human hand is typically capable of tasks with various grasp types, such as non-prehensile pushing, prehensile power grasping, and precision prismatic pinching (Dollar, 2014; McPherson et al., 2020). Hand function impairment could happen in patients due to traumas and injuries, such as spinal cord injury (SCI), stroke attacks, degenerative disease, muscle weakness due to aging, and accidents (Grefkes and Fink, 2020; Song et al., 2022). For a patient with SCI, tetraplegia with severely diminished hand function could occur. In this case, patients cannot voluntarily move their wrist joints. They only have a limited range of motion (ROM) and often lack finger movement (Howell, 2019). Stroke patients usually show upper motor neuron syndrome symptoms which include agonist and antagonist contraction, weakness, and lack of coordination. Due to these problems, stroke survivors may have a higher risk of developing spasticity in the hand and arm contractures of the wrist and finger flexor muscles (Yang et al., 2021). Rehabilitation programs for patients with impaired hand function are done at rehabilitation clinics. The problem faced by many countries with significant populations is the limited number of

therapists and rehabilitation clinics (Tulaar et al., 2017; Widagdo et al., 2021). Various hand orthoses for patients with impaired hand function are available in the market, such as wrist-driven orthosis and finger orthosis. These assistive devices improve the upper limb motor function and help establish the patient's ability to perform ADLs independently. It also reduces pain, improves strength, increases range of movement, protects from reinjury, and helps to correct any deformation (Howell, 2019). Other than orthoses, there are several device and technology developments tested for wrist rehabilitation robots such as HEXORR (Schabowsky et al., 2010) and MIT-MANUS (Krebs et al., 2007). However, those devices are bulky, causing a problem when we want to install it in health facilities around remote areas.

Regarding orthoses, they are typically characterized by their smaller sizes, particularly those designed for the upper extremities. Orthoses can be broadly classified into two categories: static and dynamic. Static orthoses are primarily focused on stabilizing and providing support to muscles and bones, which is beneficial for addressing stiff joints, joint contractures, and pain relief (Schwartz, 2012; Andringa et al., 2013). Conversely, dynamic orthoses are engineered to assist specific movements, offering support to joints, and aiding in the prevention of reinjury. They are particularly useful in cases where mobility has been compromised due to injury or illness (Andringa et al., 2013; Kang et al., 2013; Ates et al., 2015). An example of a dynamic orthosis is the passive wrist-driven hand orthosis (D-WDO), which relies on a mechanical structure to enable stronger wrist muscles to control weaker hand muscles (Amirabdollahian et al., 2014; Ates et al., 2014). While prefabricated passive D-WDOs are widely available, they may lack customization and adaptability to individual needs, which is essential for optimal rehabilitation (Howell, 2019).

Currently, 3D printing technology allows accurate D-WDO fabrication through CAD software. Using 3D printing technology, passive D-WDO can be designed to be modular and customizable, allowing for adjustments for the individual's specific needs. Some researchers have also proposed the design under an open-source license allowing anyone to modify and improve the designs. Portnova et al. has proposed a passive D-WDO designed under an open-source license with a modular concept. The passive D-WDO proposed in (Portnova et al., 2018a) was mainly designed for SCI patients at the 6th-7th cervical levels with wrist extensor strength of grade 3 or above on the manual muscle test (MMT). However, a patient may lack voluntary wrist extension and hand motion, especially those with muscle strength grades of 2–3 on the manual muscle test (MMT).

To improve strength and coordination between wrist muscles and hand motion, a passive D-WDO may be modified to mimic repetitive motion exercises of hand therapy. Some modifications to the passive D-WDO structure were made to give new functions to the passive D-WDO, such as adding an actuator component and motion control system. Several types of active actuators could be used for active D-WDO, electromechanical actuators such as motors with bar or cable transmission and linear actuators (Ochoa et al., 2011; Gopura et al., 2016; McPherson et al., 2020). These actuators typically consist of an electric DC motor, a gearbox, and a mechanism for converting rotary to linear motion. The structure of the electromechanical actuators itself is rigid and heavy, making it relatively harder to customize for the open-source D-WDO that is fabricated using 3D printing. Another type of actuator employs air pressure signals, or pneumatic input, to drive the system. Thus, in the last 2 decades, many researchers have focused on developing a pneumatic actuator that is based on soft materials, known as Soft Pneumatic Actuator (SPA) (Ang and Yeow, 2019; J; Wang et al., 2019). Because of its flexibility and bending ability, SPA can also be designed with a specific structure to function as a linear and rotary actuator. Many has developed active D-WDO with soft actuators, such as fabric-based wrist brace with origami-like actuators (Liu et al., 2021), fabric-based support splint with McKibben Muscle (Sasaki et al., 2005), or metal-structured orthosis with soft actuators (Tsagarakis and Caldwell, 2003). However, there has been limited development of rigid-structured D-WDO systems that employ a primary actuator in the form of a 3D-printed soft pneumatic actuator which enables operation with or without the actuator.

Thus, this work proposed a dual-mode D-WDO designed to perform exercises in passive and active modes. The generated motion was focused on the wrist flexion-extension, then transmitted into the palm. In active mode, the D-WDO is attached to a modular SPA, performing repetitive wrist exercises controlled with an electro-pneumatic air pressure system. The active D-WDO could be easily switched between active to passive modes simply by attaching or removing the SPA from the D-WDO structure. With follow concept of open-source orthotics, the D-WDO structure and SPA were designed using CAD software. Then, it was fabricated using a fused deposition modeling (FDM) 3D printer. A single-camera motion tracking system was used for ROM evaluation of wrist flexion and extension during active D-WDO operation. This paper is organized as follows: section 2 describes the materials and methods, section 3 describes the experiment study, section 4 results and discussion, and Section 5 describes the conclusion.

2 Materials and methods

2.1 Main structure of dynamic wrist-driven hand orthosis (D-WDO)

Passive D-WDO is an assistive device for promoting functional hand and improving muscle strength of tenodesis grasp for patients with tetraplegic SCI. The use of passive D-WDO is limited to patients with the ability to move the wrist and hand throughout the range of motion, either against gravity or by maintaining the testing position (this shows that the patient's grades of MMT are above 3). The typical passive D-WDO based on the open-source design shown in Figure 1 was not applicable for patients with no ability to move the wrist and palmar throughout the normal range of motion and only maintain the testing position if the gravity was eliminated (Grades MMT of 2–3). For patients who have the potential to reach an MMT grade of 3 or above by doing therapy, repeating exercises of wrist and palmar movements may improve motor function. To support exercise programs for patients with weak muscles, an active D-WDO is required. The main structure of D-WDO must be modified from the open-source design of passive D-WDO (see Figures 1A), and a soft pneumatic actuator (SPA) was added as motion input.

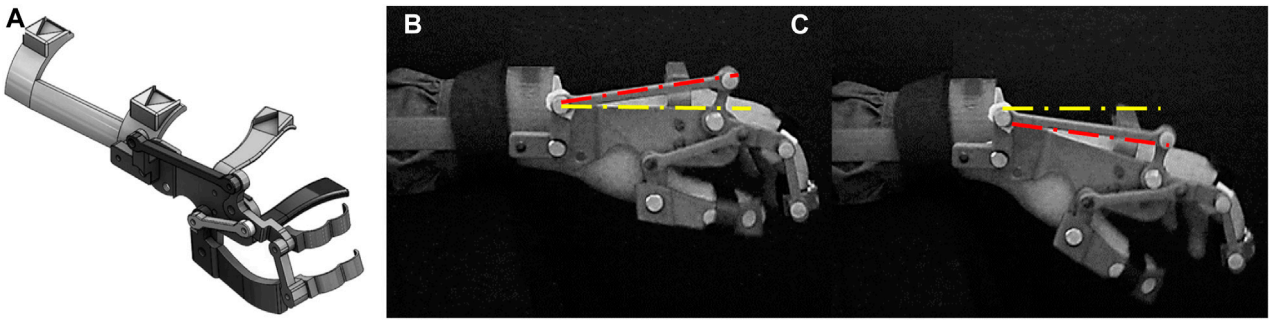

FIGURE 1
(A) The concept of passive D-WDO that was proposed in (Portnova et al., 2018a), **(B)** 3D printed passive D-WDO during wrist extension, and **(C)** during wrist flexion.

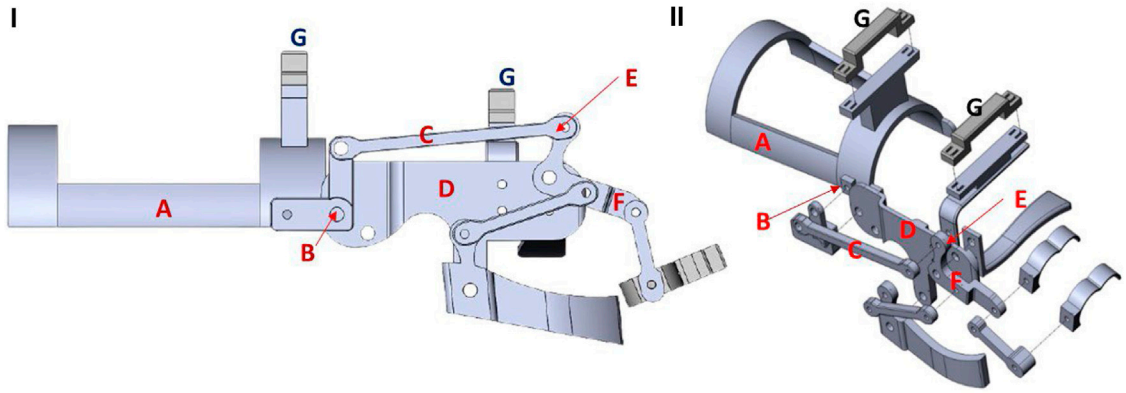

FIGURE 2
(I) The side view of modular passive D-WDO, with main components, stabilized forearm holder-**(A)**, wrist joint-**(B)**, actuating long Bar linkage-**(C)**, actuating palm bar linkage-**(D)**, metacarpophalangeal (MCP) Joint-**(E)**, operating finger Lever-**(F)** and SPA mounting-**(G)** (II) Exploded view of the D-WDO structure.

The structure of D-WDO consists of several parts, which include a stabilized forearm holder, actuating long and palm bar linkage, and operating finger lever. The wrist and metacarpophalangeal (MCP) joint were provided for a pivot rotation movement. The D-WDO structure design allows the wrist muscle to drive flexion and extension of the hand palm, and the long bar linkage transmits the motion (Kang et al., 2013; Portnova et al., 2018b). The proposed design modification for passive D-WDO was by adding SPA mounting, shown in Figure 2.

The D-WDO structure underwent modifications using computer-aided design (CAD) software, with a specific focus on enhancing the stability of the forearm holder and optimizing the actuating palm bar linkage. In the forearm holder, a SPA mounting was introduced. The primary aim of these modifications was to facilitate swift SPA installation and removal using basic tools, achieved by clamping both ends of the SPA to the mounting (as illustrated in Figure 2G). The design was subsequently 3D-printed using the FDM Creality CR10 V3 with direct drive extruder which capable of printing various materials, including PLA, ABS (Acrylonitrile Butadiene Styrene), PETG (Polyethylene Terephthalate), and TPU.

In order to induce wrist extension, it is necessary to shorten the SPA's length from L_0 to L_E, as depicted in Figure 3I. This adjustment entails applying a negative air pressure input to contract the SPA from its initial length (L_0) to the desired length (L_E). During wrist extension, the wrist

Angle transitions from θ_i to θ_E as shown in Figures 3 I, II. Conversely, to facilitate wrist flexion, the wrist angle must transition from θ_i to θ_F. This necessitates the SPA to elongate, expanding its length from L_o to L_F (see Figures 3 I, III). Before embarking on the design of the SPA, a specific deformation characteristic was set as the primary requirement. The SPA needed to be able to possess the capability to simultaneously contract, elongate, and exhibit a slight bending, all in response to the pressure input. Among the prominent SPA design types, two noteworthy options are the Fiber-reinforced actuator and the pneumatic network (Pneu-Net) actuator (Sun et al., 2019).

A fiber-reinforced SPA is an actuator that uses pressurized air to drive motion. It is made of an elastomer body with a single central chamber. The type of SPA contains helically arranged fibers on the surface that provide additional strength and protect the actuator from excessive deformation. Fiber-reinforced soft actuators can

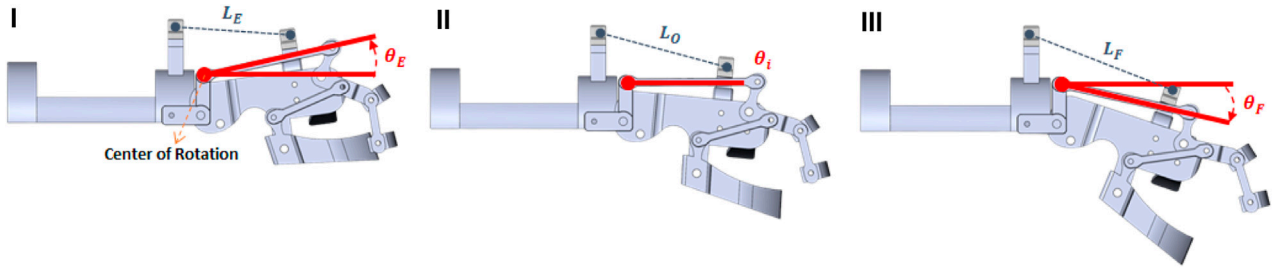

FIGURE 3
The mechanism of active D-WDO to assist repetitive movement of the wrist on three positions, i.e., extension (I), initial (II), and flexion (III).

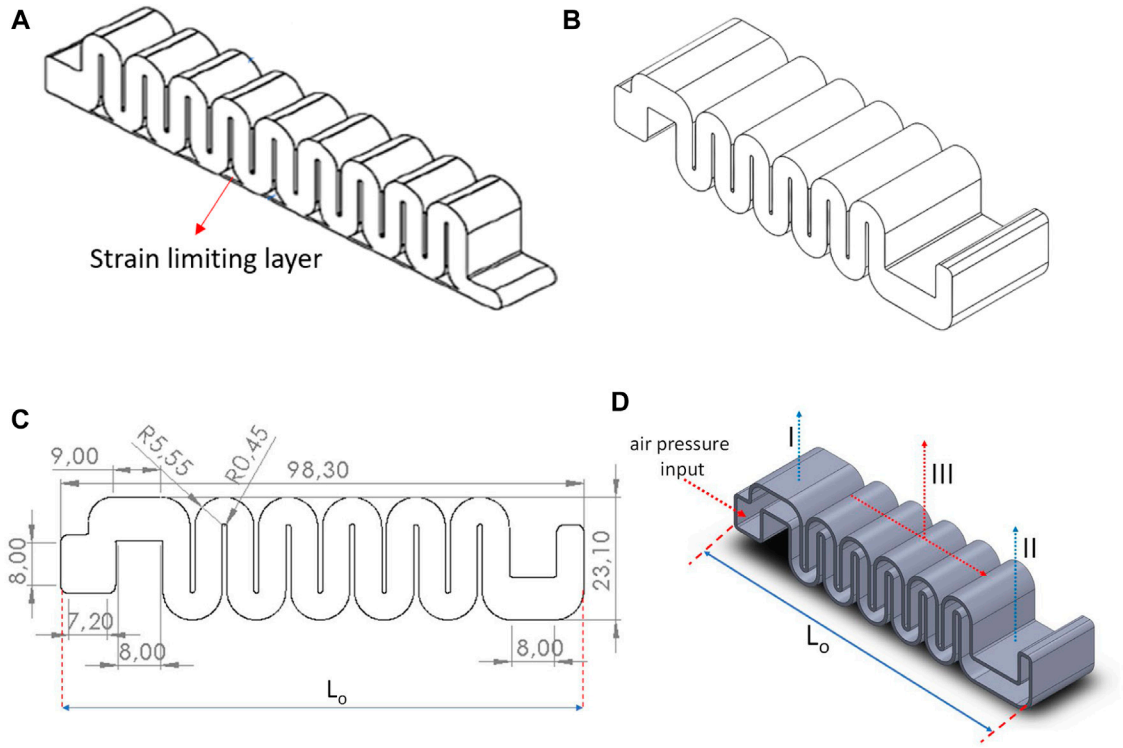

FIGURE 4
(A) Conventional bending Pneu-Net with strain limiting layer, **(B)** Modified Pneu-Net with a corrugated **(C)** Side view, unit representation in mm and L_o is the initial distance between both SPA mountings, **(D)** Slice view: 3D visualization on the inner view of modification single-chamber Pneu-Net, which consists fixed chamber (denoted I and II) of the SPA on the actuator mounting and the five compartments of the active chamber (III).

undergo large deformations due to their soft and flexible nature. They can stretch, bend, twist, and compress, allowing for a wide range of motion. The fabrication of fiber-reinforced SPA is commonly using an injection of soft material such as silicone or elastomer into specific design molding (Polygerinos et al., 2015; Wirekoh et al., 2021; Sun et al., 2022; Wei et al., 2022). A Pneu-Net actuator comprises a soft material body with interconnected pneumatic channels and small chambers (Manns et al., 2018; Sun et al., 2019; Gu et al., 2021). These chambers will define the deformation of the actuators due to pressurized air input. A Pneu-Net can be built by using a single chamber structure (Ang and Yeow, 2019; Stano et al., 2020; Rad et al., 2022) or multi-chambers connected by channels (Sun et al., 2019; J; Wang et al., 2019; Z; Wang and Hirai, 2017). The advantage of a single-chamber Pneu-Net soft actuator is its simplicity of fabrication compared to more complex multi-chamber systems. The motion characteristic of a Pneu-Net SPA is controlled by modifying the chambers' geometry and their walls' material properties. Small chambers inside a SPA could achieve bending and twisting motions when inflated by altering the angle. The air volume inside a single chamber Pneu-Net is proportional to its range of motion and strength.

A single chamber Pneu-Net could be fabricated using a fused deposition modeling (FDM) 3D printer with elastic filaments (Garcia Morales et al., 2020; Xavier et al., 2021). The typical

TABLE 1 The main slicing parameters for 3D printed SPA using TPU 95A filament.

Parameters	Setting values
Extruder and bed temperature	230°C and 60°C
Interior fill percentage	100%
External fill pattern	rectilinear with angle offsets 45° and −45°
Outline overlap	50%
Extrusion width	0.42 mm
Retraction distance	2 mm
Retraction speed	25 mm/s
Primary layer height	0.12 mm
Default printing speed	30 mm/s
Movement behaviour: Avoid crossing outline for travel movements. Maximum allowed detour factor *Thin wall behaviour:*	100
External thin wall type	Perimeters only
Internal thin wall type	Allow gap fill
Allowed perimeter overlap	15%
Printing time	7 h 57 min

structure of a conventional 3D-printed Pneu-Net includes a strain-limiting layer on the bottom layer under the SPA's chambers (see Figure 4A). A SPA will produce a bending motion rather than extending along the structure direction by utilizing this structure. The conventional Pneu-Net is mainly developed for hand glove rehabilitation (Low et al., 2015; Ang and Yeow, 2019; Guo et al., 2020). To drive movement on the long bar linkage, the conventional SPA design must be modified to fulfill the requirement as follows, during the initial condition, the air pressure input is 0 kPa, the length of the SPA that was clamped on the mounting was L_o, and the initial angle that was measured from the MCP joint relative to the wrist joint was defined as θ (see Figures 3II). Then the supplied pressure input will drive changes in the SPA dimension, which is an elongation during a positive pressure supply and compression during a negative pressure supply.

The first modification is removing the bottom strain-limiting layer on the single-chamber Pneu-Net. Then, the chamber was split into an interconnected series of fixed and flexible chambers to support the SPA function in active D-WDO. The illustration of the modified single-chamber Pneu-Net with the removed bottom strain-limiting layer actuator is shown in Figure 4. The fixed chambers were placed on both ends of the SPA and intended for the SPA installation on the mounting. While the flexible chamber was not fixed on any parts of the D-WDO structure, allowing extension and compression of the SPA structure. This modification allows the SPA to drive motion when pressure input is applied.

For practicality in D-WDO fabrication, the FDM 3D printer was used to print the structure of D-WDO (see Figure 2) and SPA (see Figures 4D). The polylactide acid (PLA) filament was used for the orthosis structure. We followed standard parameters for printing in FDM 3D printers since the filament was commonly used for many applications. However, the Pneu-Net SPA fabrication was challenging since the printing parameters must be customized based on an elastic material. The Pneu-Net SPA was printed using the eSun Thermoplastic Polyurethane (TPU) filament with a shore hardness of 95A. The 3D printer was equipped with a direct drive extruder to minimize clogging during the printing process. The optimal wall thickness of the chamber must be chosen to avoid holes in the wall structures of the SPA during the fabrication process, which might cause a pressure leakage.

The primary requirement for this component is to eliminate any holes in the wall structures of the Soft Pneumatic Actuator (SPA) to prevent air leakage and ensure an airtight inner chamber. We experimented with wall thickness ranging from 0.70 mm to 1.10 mm, with 0.1 mm increments, to create a leakage-free SPA capable of withstanding a maximum air pressure of 200 kPa. The SPA was printed in various orientations on the print bed to identify the most effective printing method and prevent leaks. Using the Simplify3D slicer, we summarized the key slicing parameters for printing the SPA using TPU 95A in Table 1. In the Simplify3D slicer, the SPA is positioned in the center of the printing bed with an upright orientation and supports are added to ensure the successful printing of overhanging structures or islands. This approach results in a ready-to-use SPA that does not require additional treatment to minimize leaks. Following the initial testing of the fabricated SPA, we found that the SPA with a wall thickness of 1.10 mm was capable of withstanding a maximum pressure supply of 200 kPa without any leakage during pressurization.

The deformation comparison of conventional Pneu-Net and modified Pneu-Net due to 200 kPa of air pressure input is shown in Figure 5. From these results, the modified single-chamber Pneu-Net

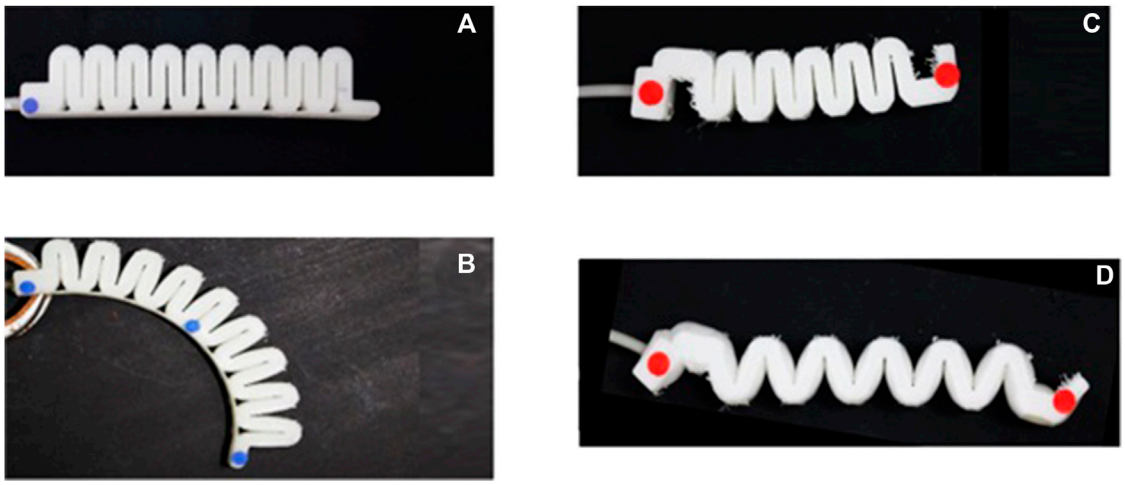

FIGURE 5
(A) conventional Pneu-Net initial condition and **(B)** deformed condition when subjected to air pressure of 200 kPa. **(C)** modified Pneu-Net initial condition and **(D)** deformed condition when subjected to air pressure of 200 kPa.

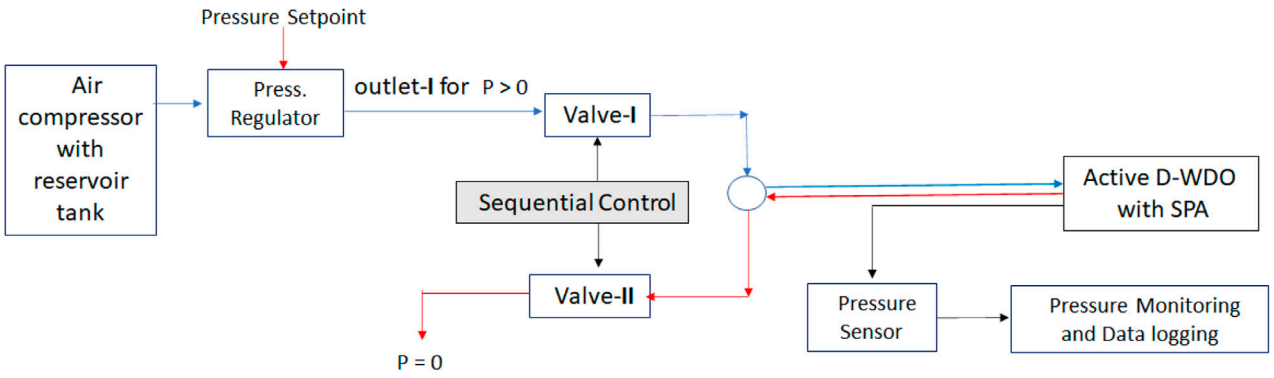

FIGURE 6
Block diagram of the first electro-pneumatic system setup: with air compressor.

shows that it can generate a deformation according to the requirement of the active D-WDO system. Then, the fabricated SPA was mounted on the D-WDO structure.

2.2 Supporting system of active (D-WDO) for performing repetitive wrist movement

The proposed supporting system consists of an electro-pneumatic system, and a camera-based motion tracking system was implemented to drive the active D-WDO and its evaluation. The primary purpose of the electro-pneumatic system was to apply a repetitive movement scheme of the wrist by controlling the air pressure supplied to the SPA. The component in the electro-pneumatic system consists of an air pressure supply, pneumatic tubes, a pressure sensor, solenoid valves, a pressure regulator, and a control system. The pressure sensor monitors the pressure inside the SPA when the active D-WDO system is operated.

In the first setup (see Figure 6), an air compressor with a reservoir tank was used to supply positive pressurized air with a maximum of 1,000 kPa into the SPA. However, due to SPA's limited working pressure, the maximum pressure output is limited to 200 kPa by using a pressure regulator. On the first experiment setup, on the initial condition, the control system commands closing both valve-I and II, resulting in a normal wrist position which has an angle of θ_i. The sequential control gives commands to open Valve-I and close Valve-II within a specific duration. In this state, a pressurized airflow was utilized to drive wrist flexion (θ_i to θ_F). For the next phase, the control system commands the closing of Valve-I and the opening of Valve-II which resulted in the pressure release from the SPA to the atmosphere. Then, due to the SPA stiffness, the wrist angle of the structure will return to its initial position.

In the second experiment setup, an electro-pneumatic system with a 12 VDC diaphragm air pump was used to supply both positive and negative pressure air flow into the SPA. In this second

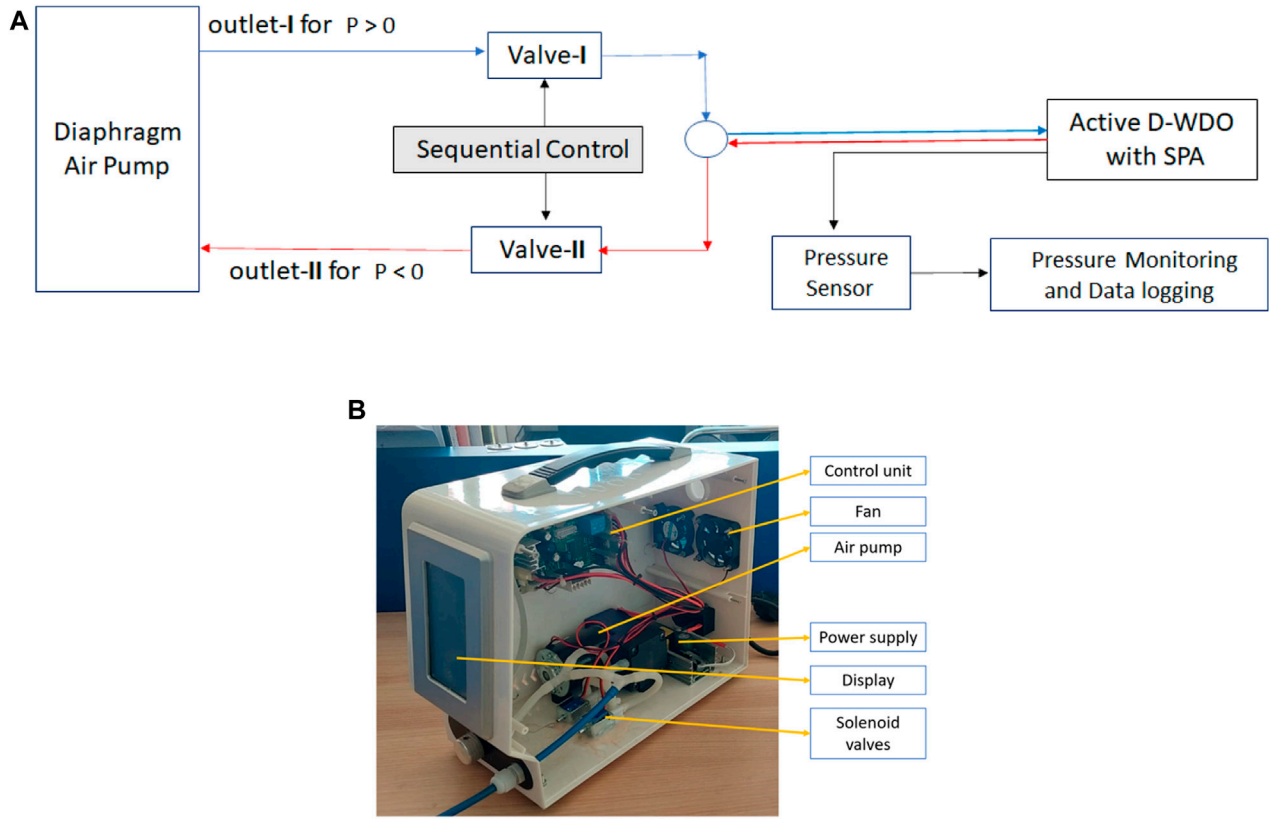

FIGURE 7
(A) Block diagram of the second electro-pneumatic system setup: with air pump, **(B)** the second system's components.

setup, the system was designed as a portable device to make it accessible for more people. The block diagram of the second experiment setup is shown in Figure 7. On the second experiment setup, the control system commands the closing of both Valve-I and II, resulting in an initial wrist position that has an angle of θ_i. The control system then commands to open Valve-I and close Valve-II to drive the wrist flexion (θ_i to θ_F). Positive air pressure drives the SPA to extend and bend simultaneously. The control system then commands the opening of Valve-II and the closing of Valve-I to convert the wrist position from flexion to extension (θ_F to θ_E). During this condition, the air pump will supply negative pressure to the SPA, shortening the SPA's length and resulting in wrist extension. The electro-pneumatic system with air pump is as shown in Figure 7B.

3 Experiment

The proposed dual-mode D-WDO was designed to operate in passive and active modes with the same orthosis structure. The D-WDO mode was determined by utilizing both the SPA and electro-pneumatic system. Without the SPA, the mode was set to passive, where D-WDO will assist functional hands and improve muscle strength for stronger patients. The mechanical structure of D-WDO could drive changes in wrist angle and control motion on palmar and fingers, enabling the wearer to grasp and release objects easily. For patients who lack voluntary wrist movement, passive D-WDO can be transformed into an active orthosis therapy device by attaching the SPA to the D-WDO structure and integrating the structure with the electro-pneumatic system. The proposed system used active D-WDO to improve muscle strength and coordination, especially between wrist and hand muscles. The illustration of the proposed dual-mode D-WDO system is shown in Figure 8.

The modified Pneu-Net SPA performance, when operated in active mode, was evaluated when the system performed repetitive movement exercises during the therapy simulation. The performance evaluation protocol of the active D-WDO is as follows: a healthy volunteer with the equivalent size of forearm and palmar was fitted to the rigid structure of D-WDO. The subject was seated on the chair with their arms on the armrest. They were asked to relax their arms and hands and let the active D-WDO drive the motion in their wrist and hands. The motion was derived from the attached SPA, driven by the electro-pneumatic system. A simple motion tracking system with a single camera was used to evaluate the motion generated by the active D-WDO during repetitive wrist movement—a DSLR Canon EOS 550D, which allows video recording at 50 fps, was used for wrist movement evaluation. The camera was positioned in front of the active D-WDO system, and it must cover all the active D-WDO parts, including the passive markers, which were placed on both ends of the long bar linkage. Then, the derived angle θ was calculated from the detected marker's position.

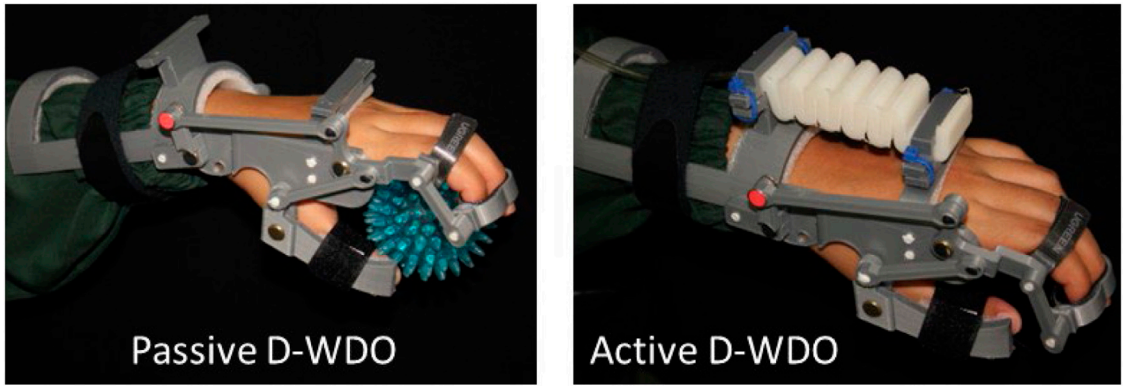

FIGURE 8
Dual mode D-WDO: (left) passive mode and (right) active mode with the same orthosis structure.

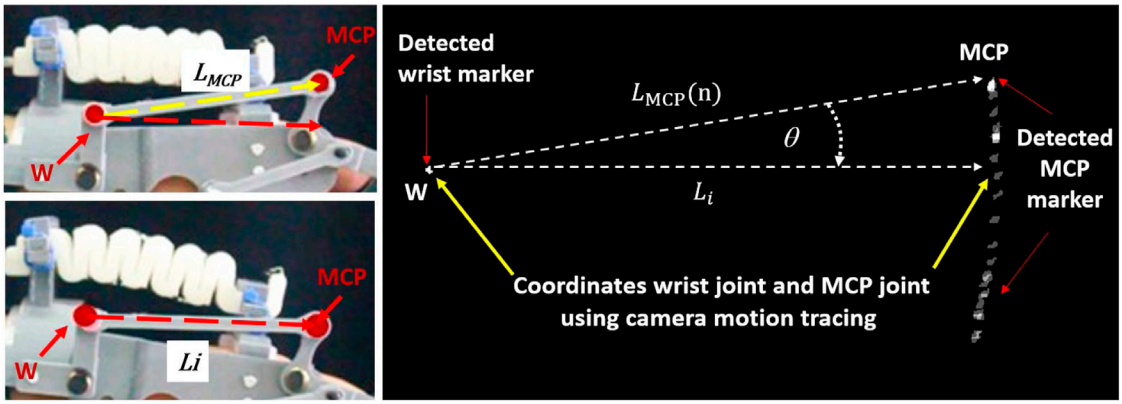

FIGURE 9
Wrist angle θ estimation from detected marker.

Red passive markers with a diameter of 5 mm (about 0.2 in) were placed on both ends of the long bar linkage to estimate the wrist angle. The markers represented the wrist and MCP joint, as Figure 9 (left) illustrates. Their image sequence was then analyzed in the recorded video. Color channels separated the images to determine the marker color significance. Then, further image processing steps, such as filtering, thresholding, and image morphology calculations, were performed in every image in the recorded video. This process will produce images showing only the marker's position detected in every frame. Figure 9 (right) shows the result of the wrist and MCP marker's position sequence in a single image, from the initial condition to flexion and extension.

Before calculating the wrist angle, the wrist angle θ will be defined as the angle between L_i and $L_{MCP}(n)$, where L_i is the line between the wrist and MCP marker in the first frame (initial condition) and $L_{MCP}(n)$ is the line between the wrist and MCP marker in the subsequent frames. Define vector $\vec{L_i} = \{x_i\vec{a_x}, y_i\vec{a_y}\}$, where x_i and y_i are vector magnitude on x and y vector direction, and $\vec{L_{MCP}} = \{x_{MCP}\vec{a_x}, y_{MCP}\vec{a_y}\}$, where x_{MCP} and y_{MCP} are vector magnitude on x and y vector direction. To calculate θ, first, the angle of L_i (see Eq 1) and $L_{MCP}(n)$ (see Eq 2) was calculated with regards to the x-axis, the angle difference between L_i and $L_{MCP}(n)$ is defined as wrist angle $\theta(n)$.

$$\angle L_i = \tan^{-1}\left(\frac{y_i}{x_i}\right) \tag{1}$$

$$\angle L_{MCP}(n) = \tan^{-1}\left(\frac{y_{MCP}(n)}{x_{MCP}(n)}\right) \tag{2}$$

$$\theta(n) = \angle L_{MCP}(n) - \angle L_i \tag{3}$$

Then, the wrist angle $\theta(n)$ was analyzed by its relationship with the supplied pressure as a function of time.

4 Results and discussion

Using the air compressor system setup (see Figure 6), the range of wrist angle during flexion phase when the motion was derived from the active D-WDO (see Figure 8-Right) was evaluated. The system was set to perform a repetitive movement using three maximum pressure values, i.e., 100 kPa, 150 kPa, and 200 kPa. The sequence control was programmed to execute five cycles of

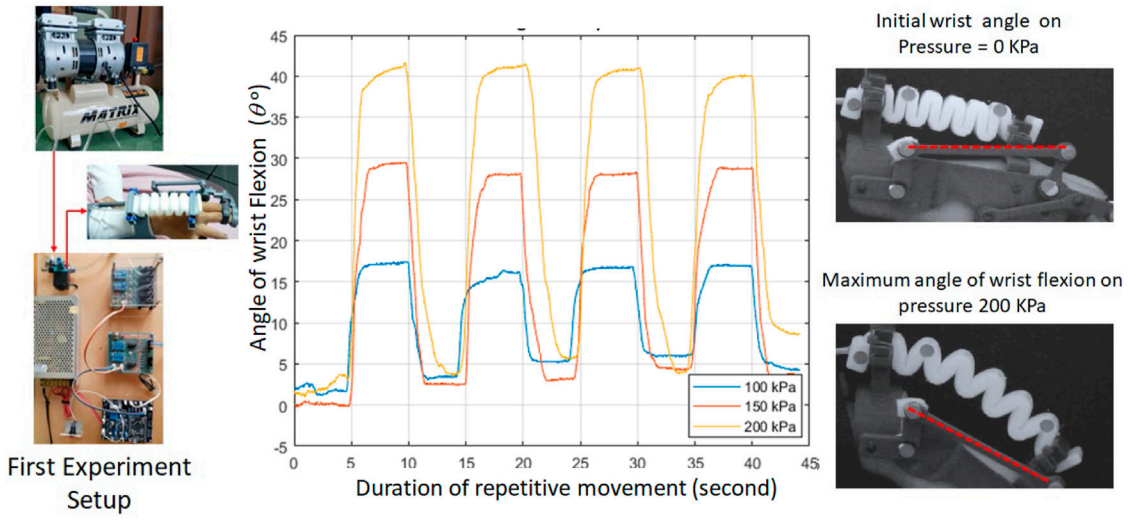

FIGURE 10
The wrist angle shift of active D-WDO system with the first experiment setup (air compressor) with pressure value of 100 kPa, 150 kPa, and 200 kPa.

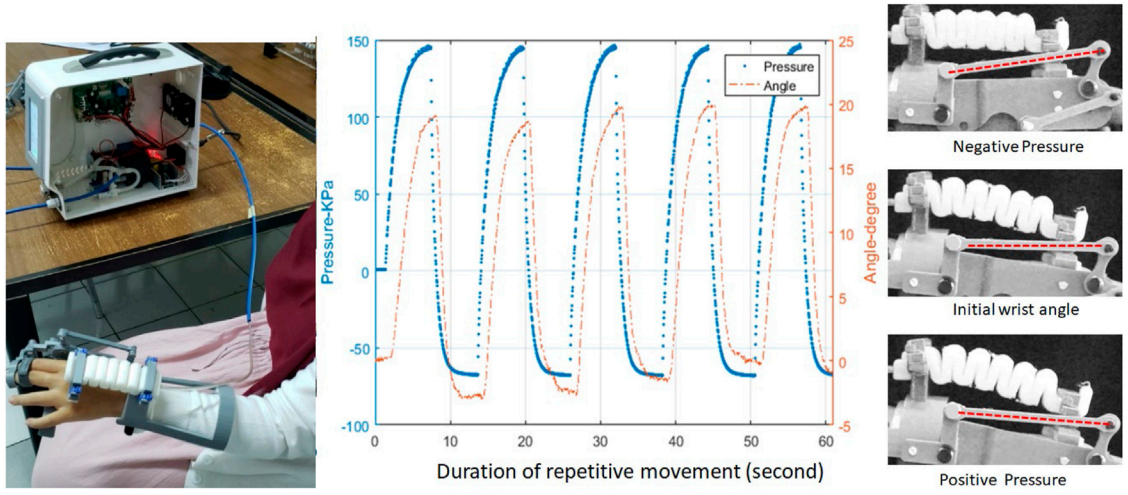

FIGURE 11
The wrist angle shift for the second experiment setup: air pump.

wrist flexion movement, where positive pressure air flow was given for 6 s alternately, with a total duration of roughly 45 s. Based on the camera-based motion tracking system, the change of $\theta(n)$ for the five cycles of repetitive movement on each pressure setpoints value is shown in Figure 10. The maximum angle of wrist flexion for each airflow pressure of around 100 kPa, 150 kPa, and 200 kPa was found at 17.41°, 26.32°, and 41.62°, respectively.

However, there are limitations to the first experiment setup, which causes significant drawbacks. There are two major drawbacks: 1) its inability to serve as a portable system because of the compressor utilization and 2) its inability to give negative pressure supply causing a limited system function. The first setup causes the system to perform wrist flexion exclusively. Then the structure returns to the initial condition by acquiring the SPA's stiffness property which tends to regain its original shape when not pressurized. Based on the five-cycle movement, the average value of the initial wrist angle of the first experiment setup was 3.45° ± 3.30° (see Figure 10).

The next evaluation was for active D-WDO system when air pump was utilized as the main air supply component. By utilizing the air pump, the whole system was able to be operated as a portable system. As described in the previous section (see Figure 7), the air pump operating pressure range was [-60 kPa, 140 kPa]. Four healthy (n = 4) volunteers were involved during the performance evaluation of the active D-WDO system. Based on the camera-based motion tracking system, the shift of wrist

angle $\theta(n)$ with regards to the supplied air pressure is shown in Figure 11. The average maximum wrist flexion angle when the air pump supplies a positive pressure for five cycles was 19.28° ± 1.44° (n = 4). When the negative pressure from the air pump occurred, the air volume on the SPA chamber drastically decreased. During this condition, the length of the active chamber SPA (see Figure 5) was also decreased, resulting in a wrist extension. The average wrist extension angle for five cycles was −7.68° ± 1.95° (n = 4). As shown in Figure 11, we can see that the pneumatic system is much smaller than when the air compressor is utilized since the air pump is placed inside the panel. Thus, producing a portable pneumatic system for the D-WDO system.

Based on the performance evaluation of active D-WDO system that was driven by the air compressor and the air pump, the D-WDO could reach a maximum wrist flexion angle of 41° and 19°, respectively. However, the wrist might be flexed to more than 40° in common therapy exercises which might not be applicable for patients with muscle spasticity (Ates et al., 2014). Figure 10 and Figure 11 reveal a consistent flexion angle in both setups. Specifically, the generated wrist flexion angle remains similar when the actuator is pressurized to approximately 150 kPa, irrespective of the pneumatic system setup. It is essential to acknowledge that achieving an exact pressure value of 150 kPa from the air compressor was challenging due to manual control using a manual regulator. When compared to the setup employing air pumps, it becomes evident that the air pump generates a lower pressure value than the air compressor, consequently leading to a reduced wrist flexion angle. However, the generated wrist angle was able to reach the required wrist flexion angle when it was supplied with an air pressure input value of 200 kPa. The 3D-printed modified Pneu-Net SPA has also shown the capability to drive active D-WDO system and perform repetitive wrist exercises. The active chamber in the proposed SPA design also provides a sufficient pulling force on the palm bar linkage which return the D-WDO structure to its initial wrist angle when the air pressure inside the SPA was returned to the atmospheric pressure. This behavior is attributed to the stiffness properties of the SPA's material. Nonetheless, the SPA's stiffness property proves advantageous only when the air pressure supply can provide positive pressure values, as demonstrated in the results of the first experiment. In contrast, the proposed modified Pneu-Net SPA was capable of reducing its length when subjected to negative air pressure of −60 kPa, as demonstrated in the results of the second experiment, which involved the use of an air pump. In addition to evaluating the active D-WDO system, we also assessed the proposed single-camera motion tracking system. This system employs a single camera to track passive color markers attached to the D-WDO structure on the wrist and MCP joint. The graph in Figure 11 illustrates that the motion tracking system exhibited outstanding performance in tracking the positions of passive markers during the experiment.

5 Conclusion

This work discusses the development of a dual-mode dynamic wrist-driven wrist-hand orthosis (D-WDO) with a soft pneumatic actuator (SPA) as its active component. This dual-mode design introduced a system that can serve the same function for different patient conditions with the utilization of a detachable SPA. The system's mode was defined by the SPA utilization. All components in the dual-mode D-WDO system were designed and fabricated by CAD software and FDM 3D printing method. PLA and TPU filament were used for the D-WDO structure and soft actuator, respectively, to make the system customizable for various patients. The dual-mode D-WDO system can help the rehabilitation process for patients with any residual motor function level who needs a therapeutic device and could also be operated as passive and active WDO.

Data availability statement

The raw data supporting the conclusion of this article will be made available by the authors, without undue reservation.

Ethics statement

Written informed consent was not obtained from the individual(s) for the publication of any potentially identifiable images or data included in this article because the obtained images was only the hand of the participants.

Author contributions

AR: Conceptualization, Data curation, Formal Analysis, Investigation, Methodology, Validation, Visualization, Writing–original draft. SS: Writing–review and editing. YN: Writing–review and editing. AM: Writing–review and editing.

Funding

The author(s) declare that no financial support was received for the research, authorship, and/or publication of this article.

Conflict of interest

The authors declare that the research was conducted in the absence of any commercial or financial relationships that could be construed as a potential conflict of interest.

Publisher's note

All claims expressed in this article are solely those of the authors and do not necessarily represent those of their affiliated organizations, or those of the publisher, the editors and the reviewers. Any product that may be evaluated in this article, or claim that may be made by its manufacturer, is not guaranteed or endorsed by the publisher.

References

Amirabdollahian, F., Ates, S., Basteris, A., Cesario, A., Buurke, J., Hermens, H., et al. (2014). Design, development and deployment of a hand/wrist exoskeleton for home-based rehabilitation after stroke - SCRIPT project. *Robotica* 32 (8), 1331–1346. doi:10.1017/S0263574714002288

Andringa, A., Van De Port, I., and Meijer, J. W. (2013). Long-term use of a static hand-wrist orthosis in chronic stroke patients: a pilot study. *Stroke Res. Treat.* 2013, 1–5. doi:10.1155/2013/546093

Ang, B. W. K., and Yeow, C. H. (2019). "3D printed soft pneumatic actuators with intent sensing for hand rehabilitative exoskeletons," in Proceedings of the 2019 International Conference on Robotics and Automation (ICRA), Montreal, QC, Canada, 2019-May. doi:10.1109/ICRA.2019.8793785

Ates, S., Leon, B., Basteris, A., Nijenhuis, S., Nasr, N., Sale, P., et al. (2014). "Technical evaluation of and clinical experiences with the SCRIPT passive wrist and hand orthosis," in Proceedings of the 2014 7th International Conference on Human System Interactions (HSI), Costa da Caparica, Portugal, June 2014, 188–193. doi:10.1109/HSI.2014.6860472

Ates, S., Mora-Moreno, I., Wessels, M., and Stienen, A. H. A. (2015). "Combined active wrist and hand orthosis for home use: lessons learned," in Proceedings of the 2015 IEEE International Conference on Rehabilitation Robotics (ICORR), Singapore, 2015-September. doi:10.1109/ICORR.2015.7281232

Dollar, A. M. (2014). "Classifying human hand use and the activities of daily living," in *Springer tracts in advanced robotics* (Berlin, Germany: Springer). doi:10.1007/978-3-319-03017-3_10

Garcia Morales, D. S., Ibrahim, S., Cao, B. H., and Raatz, A. (2020). Design and characterization of a 3d printed soft pneumatic actuator. *Mech. Mach. Sci.* 89, 488–495. doi:10.1007/978-3-030-55061-5_55

Gopura, R. A. R. C., Bandara, D. S. V., Kiguchi, K., and Mann, G. K. I. (2016). Developments in hardware systems of active upper-limb exoskeleton robots: a review. *Robotics Aut. Syst.* 75, 203–220. doi:10.1016/j.robot.2015.10.001

Grefkes, C., and Fink, G. R. (2020). Recovery from stroke: current concepts and future perspectives. *Neurological Res. Pract.* 2 (1), 17. doi:10.1186/s42466-020-00060-6

Gu, G., Wang, D., Ge, L., and Zhu, X. (2021). Analytical modeling and design of generalized pneu-net soft actuators with three-dimensional deformations. *Soft Robot.* 8 (4), 462–477. doi:10.1089/soro.2020.0039

Guo, N., Sun, Z., Wang, X., Yeung, E. H. K., To, M. K. T., Li, X., et al. (2020). Simulation analysis for optimal design of pneumatic bellow actuators for soft-robotic glove. *Biocybern. Biomed. Eng.* 40 (4), 1359–1368. doi:10.1016/j.bbe.2020.08.002

Howell, J. (2019). "Principles and components of upper limb orthoses," in *Atlas of orthoses and assistive devices* (Amsterdam, Netherlands: Elsevier), 134–145. doi:10.1016/B978-0-323-48323-0.00012-3

Kang, Y. S., Park, Y. G., Lee, B. S., and Park, H. S. (2013). Biomechanical evaluation of wrist-driven flexor hinge orthosis in persons with spinal cord injury. *J. Rehabilitation Res. Dev.* 50 (8), 1129–1138. doi:10.1682/JRRD.2012.10.0189

Krebs, H. I., Volpe, B. T., Williams, D., Celestino, J., Charles, S. K., Lynch, D., et al. (2007). Robot-aided neurorehabilitation: a robot for wrist rehabilitation. *IEEE Trans. Neural Syst. Rehabilitation Eng.* 15 (3), 327–335. doi:10.1109/TNSRE.2007.903899

Liu, S., Fang, Z., Liu, J., Tang, K., Luo, J., Yi, J., et al. (2021). A compact soft robotic wrist brace with origami actuators. *Front. Robotics AI* 8, 614623. doi:10.3389/frobt.2021.614623

Low, J. H., Ang, M. H., and Yeow, C. H. (2015). "Customizable soft pneumatic finger actuators for hand orthotic and prosthetic applications," in Proceedings of the 2015 IEEE International Conference on Rehabilitation Robotics (ICORR), Singapore, 2015-September. doi:10.1109/ICORR.2015.7281229

Manns, M., Morales, J., and Frohn, P. (2018). Additive manufacturing of silicon based PneuNets as soft robotic actuators. *Procedia CIRP* 72, 328–333. doi:10.1016/j.procir.2018.03.186

McPherson, A. I. W., Patel, V. V., Downey, P. R., Abbas Alvi, A., Abbott, M. E., and Stuart, H. S. (2020). "Motor-augmented wrist-driven orthosis: flexible grasp assistance for people with spinal cord injury," in Proceedings of the 2020 42nd Annual International Conference of the IEEE Engineering in Medicine & Biology Society (EMBC), Montreal, QC, Canada, 2020-July. doi:10.1109/EMBC44109.2020.9176037

Ochoa, J. M., Kamper, D. G., Listenberger, M., and Lee, S. W. (2011). "Use of an electromyographically driven hand orthosis for training after stroke," in Proceedings of the 2011 IEEE International Conference on Rehabilitation Robotics, Zurich, Switzerland, July 2011. doi:10.1109/ICORR.2011.5975382

Polygerinos, P., Wang, Z., Overvelde, J. T. B., Galloway, K. C., Wood, R. J., Bertoldi, K., et al. (2015). Modeling of soft fiber-reinforced bending actuators. *IEEE Trans. Robotics* 31 (3), 778–789. doi:10.1109/TRO.2015.2428504

Portnova, A. A., Mukherjee, G., Peters, K. M., Yamane, A., and Steele, K. M. (2018a). Design of a 3D-printed, open-source wrist-driven orthosis for individuals with spinal cord injury. *PLoS ONE* 13 (2), e0193106. doi:10.1371/journal.pone.0193106

Portnova, A. A., Mukherjee, G., Peters, K. M., Yamane, A., and Steele, M. (2018b). Design of a 3D-printed, open-source wrist-driven orthosis for individuals with spinal cord injury. *PLOS ONE* 13, e0193106–e0193118. doi:10.1371/journal.pone.0193106

Rad, C., Hancu, O., and Lapusan, C. (2022). Data-driven kinematic model of PneuNets bending actuators for soft grasping tasks. *Actuators* 11 (2), 58. doi:10.3390/act11020058

Sasaki, D., Noritsugu, T., and Takaiwa, M. (2005). "Development of active support splint driven by pneumatic soft actuator (ASSIST)," in Proceedings of the 2005 IEEE International Conference on Robotics and Automation, Barcelona, Spain, April 2005, 520–525. doi:10.1109/ROBOT.2005.1570171

Schabowsky, C. N., Godfrey, S. B., Holley, R. J., and Lum, P. S. (2010). Development and pilot testing of HEXORR: hand EXOskeleton rehabilitation robot. *J. NeuroEngineering Rehabilitation* 7 (1), 36. doi:10.1186/1743-0003-7-36

Schwartz, D. A. (2012). Static progressive orthoses for the upper extremity: a comprehensive literature review. *HAND* 7 (1), 10–17. doi:10.1007/s11552-011-9380-2

Song, X., Van De Ven, S. S., Liu, L., Wouda, F. J., Wang, H., and Shull, P. B. (2022). Activities of daily living-based rehabilitation system for arm and hand motor function retraining after stroke. *IEEE Trans. Neural Syst. Rehabilitation Eng.* 30, 621–631. doi:10.1109/TNSRE.2022.3156387

Stano, G., Arleo, L., and Percoco, G. (2020). Additive manufacturing for soft robotics: design and fabrication of airtight, monolithic bending PneuNets with embedded air connectors. *Micromachines* 11 (5), 485. doi:10.3390/MI11050485

Sun, Y., Feng, H., Manchester, I. R., Yeow, R. C. H., and Qi, P. (2022). Static modeling of the fiber-reinforced soft pneumatic actuators including inner compression: bending in free space, block force, and deflection upon block force. *Soft Robot.* 9 (3), 451–472. doi:10.1089/soro.2020.0081

Sun, Y., Zhang, Q., Chen, X., and Chen, H. (2019). An optimum design method of pneu-net actuators for trajectory matching utilizing a bending model and ga. *Math. Problems Eng.* 2019, 1–12. doi:10.1155/2019/6721897

Tsagarakis, N. G., and Caldwell, D. G. (2003). Development and control of a 'soft-actuated' exoskeleton for use in physiotherapy and training. *Aut. Robots* 15 (1), 21–33. doi:10.1023/A:1024484615192

Tulaar, A. B. M., Karyana, M., Wahyuni, L. K., Paulus, A. F. S., Tinduh, D., Anestherita, F., et al. (2017). People with spinal cord injury in Indonesia. *Am. J. Phys. Med. Rehabilitation* 96 (2), S74–S77. doi:10.1097/PHM.0000000000000660

Wang, J., Fei, Y., and Pang, W. (2019). Design, modeling, and testing of a soft pneumatic glove with segmented PneuNets bending actuators. *IEEE/ASME Trans. Mechatronics* 24 (3), 990–1001. doi:10.1109/TMECH.2019.2911992

Wang, Z., and Hirai, S. (2017). Soft gripper dynamics using a line-segment model with an optimization-based parameter identification method. *IEEE Robotics Automation Lett.* 2 (2), 624–631. doi:10.1109/lra.2017.2650149

Wei, Q., Xu, H., Sun, F., Chang, F., Chen, S., and Zhang, X. (2022). Biomimetic fiber reinforced dual-mode actuator for soft robots. *Sensors Actuators A Phys.* 344, 113761. doi:10.1016/j.sna.2022.113761

Widagdo, T. M. M., Robot, M. M., and Pinzon, R. T. (2021). Independence in activities of daily living and quality of life of community-dwelling persons with paraplegia in Indonesia. *Int. J. Disabil. Hum. Dev.* 20 (3).

Wirekoh, J., Parody, N., Riviere, C. N., and Park, Y. L. (2021). Design of fiber-reinforced soft bending pneumatic artificial muscles for wearable tremor suppression devices. *Smart Mater. Struct.* 30 (1), 015013. doi:10.1088/1361-665X/abc062

Xavier, M. S., Tawk, C. D., Yong, Y. K., and Fleming, A. J. (2021). 3D-printed omnidirectional soft pneumatic actuators: design, modeling and characterization. *Sensors Actuators A Phys.* 332, 113199. doi:10.1016/j.sna.2021.113199

Yang, Y. S., Tseng, C. H., Fang, W. C., Han, I. W., and Huang, S. C. (2021). Effectiveness of a new 3d-printed dynamic hand–wrist splint on hand motor function and spasticity in chronic stroke patients. *J. Clin. Med.* 10 (19), 4549. doi:10.3390/jcm10194549

Zheng, J. Z., Rosa, S. D.La, and Dollar, A. M. (2013). An investigation of grasp type and frequency in daily household and machine shop tasks joshua. *IEEE Trans. Haptics* 6 (3). doi:10.1109/ICRA.2011.5980366